JACS
JOURNAL OF THE AMERICAN CHEMICAL SOCIETY
Article
pubs.acs.org/JACS

Effective Detection of Mycotoxins by a Highly Luminescent Metal–Organic Framework

Zhichao Hu,[†,∥] William P. Lustig,[†,∥] Jingming Zhang,[†] Chong Zheng,[‡] Hao Wang,[†] Simon J. Teat,[§] Qihan Gong,[†] Nathan D. Rudd,[†] and Jing Li*[,†]

[†]Department of Chemistry and Chemical Biology, Rutgers University, 610 Taylor Road, Piscataway, New Jersey 08854, United States
[‡]Department of Chemistry and Biochemistry, Northern Illinois University, 1425 W. Lincoln Highway, DeKalb, Illinois 60115, United States
[§]Advanced Light Source, Lawrence Berkeley National Laboratory, 1 Cyclotron Road, Berkeley California 94720, United States

Supporting Information

ABSTRACT: We designed and synthesized a new luminescent metal–organic framework (LMOF). LMOF-241 is highly porous and emits strong blue light with high efficiency. We demonstrate for the first time that very fast and extremely sensitive optical detection can be achieved, making use of the fluorescence quenching of an LMOF material. The compound is responsive to Aflatoxin B_1 at parts per billion level, which makes it the best performing luminescence-based chemical sensor to date. We studied the electronic properties of LMOF-241 and selected mycotoxins, as well as the extent of mycotoxin–LMOF interactions, employing theoretical methods. Possible electron and energy transfer mechanisms are discussed.

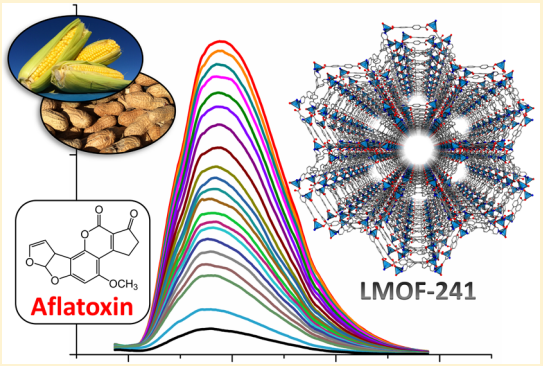

INTRODUCTION

Mycotoxins are secondary metabolites produced by certain fungi that infect and proliferate on diverse food commodities. Mycotoxins contaminate 25% of the global food crops each year, leading to the loss of 1 billion metric tons of food products annually.[1] In the U.S. alone, the economic damage caused by mycotoxins approaches $1.5 billion per year.[2] Many of these naturally occurring toxins are teratogenic, mutagenic, and carcinogenic, which pose significant adverse health effects on human beings and animals.[3]

Aflatoxins (AFs), mainly produced by *Aspergillus flavus* and *Aspergillus parasiticus*, are some of the most dominant mycotoxins worldwide.[4] AFs contaminate a wide variety of important agricultural commodities, including corn and tree nuts.[5] There are four major AFs: B_1, B_2, G_1, and G_2, of which AFB_1 is most toxic and one of the strongest known natural carcinogens. AF poisoning leads to the development of liver cirrhosis or liver cancer (hepatocellular carcinoma).[6] Ochratoxin A (OTA) produced by *Aspergillus ochraceus* and *Penicillium verrucosum* is another common mycotoxin that is hepatotoxic and nephrotoxic.[4]

The chemical stability of most mycotoxins enables their survival through various food manufacture processes such as baking and cooking at elevated temperatures, which make the prevention of their entrance into the food chain extremely difficult.[7] Therefore, monitoring mycotoxins in human foods and animal feeds is crucial to ensure food safety. The U.S. Food and Drug Administration (FDA) established the AFB_1 tolerant level for corn and peanut feeds intended for finishing beef cattle at 300 ppb.[8] Current mycotoxin detection methods focus on the use of antibodies, aptamers, immunoassays, and modern instruments (such as chromatography and mass spectroscopy), which are proven effective. However, they share some common drawbacks, such as high cost and complex sample preparation, which makes them less available to developing countries—places most prone to mycotoxin contaminations.[7] Therefore, the development of convenient, cost-effective mycotoxin detection methods has significant impact on global food safety.

Optical sensing utilizing the change in fluorescence readout induced by sensor–analyte interactions is a powerful detection method.[9] The choice of sensor material is central to achieving effective detection of the targeted analyte.[10] Metal–organic frameworks (MOFs) are a class of functional crystalline materials constructed by the self-assembly of metal nodes (metal cations or metal clusters) and organic ligands. Their tunable properties and facile characterization has made MOFs attractive materials for use in a variety of applications, including gas storage, gas separation, and catalysis.[11] Luminescent MOFs (LMOFs) are well explored as chemical sensor materials, as their easy-to-functionalize surface and tunable porosity promote feasible guest–host interactions.[12b,c] Here we demonstrate for the first time the use of a highly luminescent

Received: October 2, 2015
Published: December 11, 2015

DOI: 10.1021/jacs.5b10308
J. Am. Chem. Soc. 2015, 137, 16209–16215

LMOF for very fast and sensitive florescence-based mycotoxin detection. A detection limit of 46 ppb is reached.

EXPERIMENTAL SECTION

General Information. All reagents are used as purchased unless specified otherwise. Detailed information on sources of chemicals is in the Supporting Information (SI).

Synthesis of the tppe Ligand. Synthesis of the ligand 1,1,2,2-tetrakis(4-(pyridin-4-yl)phenyl)ethane (tppe)[13] began with the reaction of solid 1,1,2,2-tetraphenylethene (tpe) with liquid bromine to produce 1,1,2,2-tetrakis(4-bromophenyl)ethene (Br_4-tpe), which was purified via recrystallization in dichloromethane/methanol (Figure 1). A Suzuki coupling reaction between Br_4-tpe and pyridine-4-boronic

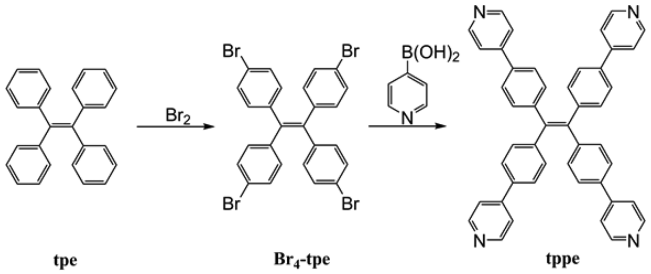

Figure 1. Synthetic scheme of tppe.

acid, catalyzed by palladium(II) acetate, was used to attach the pyridine moiety to the tpe moiety. The final product was extracted with chloroform and purified using column chromatography (stationary phase = silica, mobile phase = 30:1 $CHCl_3$/MeOH).

Synthesis of Zn_2(bpdc)$_2$(tppe) (LMOF-241). In a 20 mL glass vial, $Zn(NO_3)_2{\cdot}6H_2O$ (0.015 g, 0.05 mmol), biphenyl-4,4′-dicarboxylic acid (H_2bpdc, 0.012 g, 0.05 mmol), and tppe (0.013 g, 0.02 mmol) were added. Then *N*,*N*-dimethylacetamide (DMA, 8 mL), dimethyl sulfoxide (2 mL), and isopropyl alcohol (2 mL) were added to the mixture. The reaction mixture was kept under ultrasonication until all solids dissolved. The glass vial was sealed and kept at 150 °C for 24 h. The transparent light yellow needle-shaped crystals were harvested by filtration after the reaction mixture cooled to room temperature.

Structure Analysis of LMOF-241. Single-crystal diffraction data for LMOF-241 were collected on a Bruker APEXII CCD diffractometer using the synchrotron source (λ = 0.7749 Å) at the Advanced Light Source 11.3.1 Chemical Crystallography beamline. All non-hydrogen atoms were refined anisotropically; hydrogen atoms were placed geometrically, constrained, and refined with a riding model. The unresolvable electron density from the void space in the structure was removed by SQUEEZE. The powder X-ray diffraction (PXRD) patterns were collected on a Rigaku Ultima-IV diffractometer using monochromatic Cu Kα radiation (λ = 1.5406 Å). Data were collected between a 2θ of 3−50° with step size of 0.02° at a scanning speed of 3.0°/min (Table 1).

Porosity Characterization of LMOF-241. Gas sorption isotherms were collected on a volumetric gas sorption analyzer (Autosorb-1 MP, Quantachrome Instruments). Ultra-high-purity N_2 (99.999%) was used for the experiment. Liquid nitrogen was used as coolant to achieve cryogenic temperature (77 K). As-made LMOF-241 (200 mg) was immersed in 15 mL of dichloromethane (DCM) in a glass vial for 2 h, then the supernatant was decanted and 15 mL of fresh DCM was replenished. This process was repeated six times. About 150 mg of DCM exchanged sample was outgassed at 333 K overnight under dynamic vacuum, and the subsequent degassed sample (LMOF-241′) was used. The N_2 isotherm was collected in a pressure range from 10^{-7} to 1 atm at 77 K. Surface area was analyzed using Autosorb v1.50 software. The Brunauer−Emmett−Teller (BET) surface area of LMOF-241′ is 1268 m^2/g.

Computational Study of LMOF-241 and Mycotoxins. The electronic properties of LMOF-241 and selected mycotoxins were evaluated using extended Hückel (EH) method.[14] To quantitatively measure the interactions between LMOF-241 and Aflatoxin B_1 and B_2, simulation of mycotoxin-loaded LMOF-241 structures was performed, and configurations with closest analyte−MOF contacts were chosen for each toxin (see S9). A fragment containing a complete LMOF-241 primary building unit (PBU), composed of 1 Zn^{2+}, 2 tppe, and 2 bpdc, was used in the calculations, with dangling carboxylates terminated with hydrogen to ensure a neutral framework (see S10).

Table 1. Single-Crystal Data of LMOF-241

compound	LMOF-241
formula	$C_{111}H_{72}N_6O_{12}Zn_3$
M	1877.85
crystal system	monoclinic
space group	$C2$
a/Å	44.091(2)
b/Å	25.4060(14)
c/Å	17.1248(9)
α/deg	90
β/deg	91.176(4)
γ/deg	90
V/Å^3	19178.7(17)
Z	4
temperature/K	260(2)
λ (radiation wavelength)/Å	0.7749
D (g/cm^3)	0.650
reflections collected	83865
$R1^a$ [$I > 2\sigma(I)$]	0.0598
$wR2^b$ [$I > 2\sigma(I)$]	0.1463
goodness-of-fit	0.983
CCDC no.	1006120

$^aR1 = \sum||F_o| - |F_c||/\sum|F_o|$. $^bwR2 = \sum[w(F_o^2 - F_c^2)^2]/w(F_o^2)^2]^{1/2}$.

Optical Characterization. The optical band gap, fluorescence internal quantum yield (IQY), and solid-state excitation and emission spectra were measured for LMOF-241 at room temperature in air. Diffuse reflectance data were collected using a Shimadzu UV-3600 spectrophotometer, and the Kubelka−Munk function was used to estimate the optical band gap. IQY measurements were collected using a Hamamatsu C9220-03 spectrophotometer with integrating sphere. Solid-state excitation and emission spectra were collected using a Varian Cary Eclipse spectrophotometer.

Fluorescence Titration. Following solvent exchange with DCM to remove the solvent remaining in the structure following its synthesis, LMOF-241 was added to DCM and the mixture was kept under ultrasonication to form a suspension (4 mg/mL); stock solutions of Aflatoxin B_1 (AFB_1) Aflatoxin B_2 (AFB_2), Aflatoxin G_1 (AFG_1), and Ochratoxin A (OTA) dissolved in DCM were prepared. DCM was used as the solvent because of its photoinactivity and LMOF-241's stability in it (Figure S2). The fluorescence titration was performed by adding analyte aliquots to the LMOF-241 suspension. The initial photoluminescence (PL) spectrum of the suspension and spectra after each analyte aliquot addition were recorded on a Varian Cary Eclipse spectrophotometer. The suspension was thoroughly stirred before each PL measurement. Each measurement was repeated three times, and the average value was used.

RESULTS AND DISCUSSION

Topological Analysis. LMOF-241 or [Zn_2(bpdc)$_2$(tppe)]·S (S = guest solvent molecules) crystallizes in the monoclinic crystal system with space group $C2$. Each Zn^{2+} tetrahedrally coordinates to two monodentate carboxylates from bpdc ligands and two pyridine groups from tppe ligands, forming the PBU (Figure 2a). A hexagonal cage containing 12 Zn centers, 8 bpdc ligands, and 2 tppe ligands proliferates along the c-axis to form a one-dimensional (1D) channel; the edge-sharing channels expand into a three-dimensional (3D) net

DOI: 10.1021/jacs.5b10308
J. Am. Chem. Soc. 2015, 137, 16209−16215

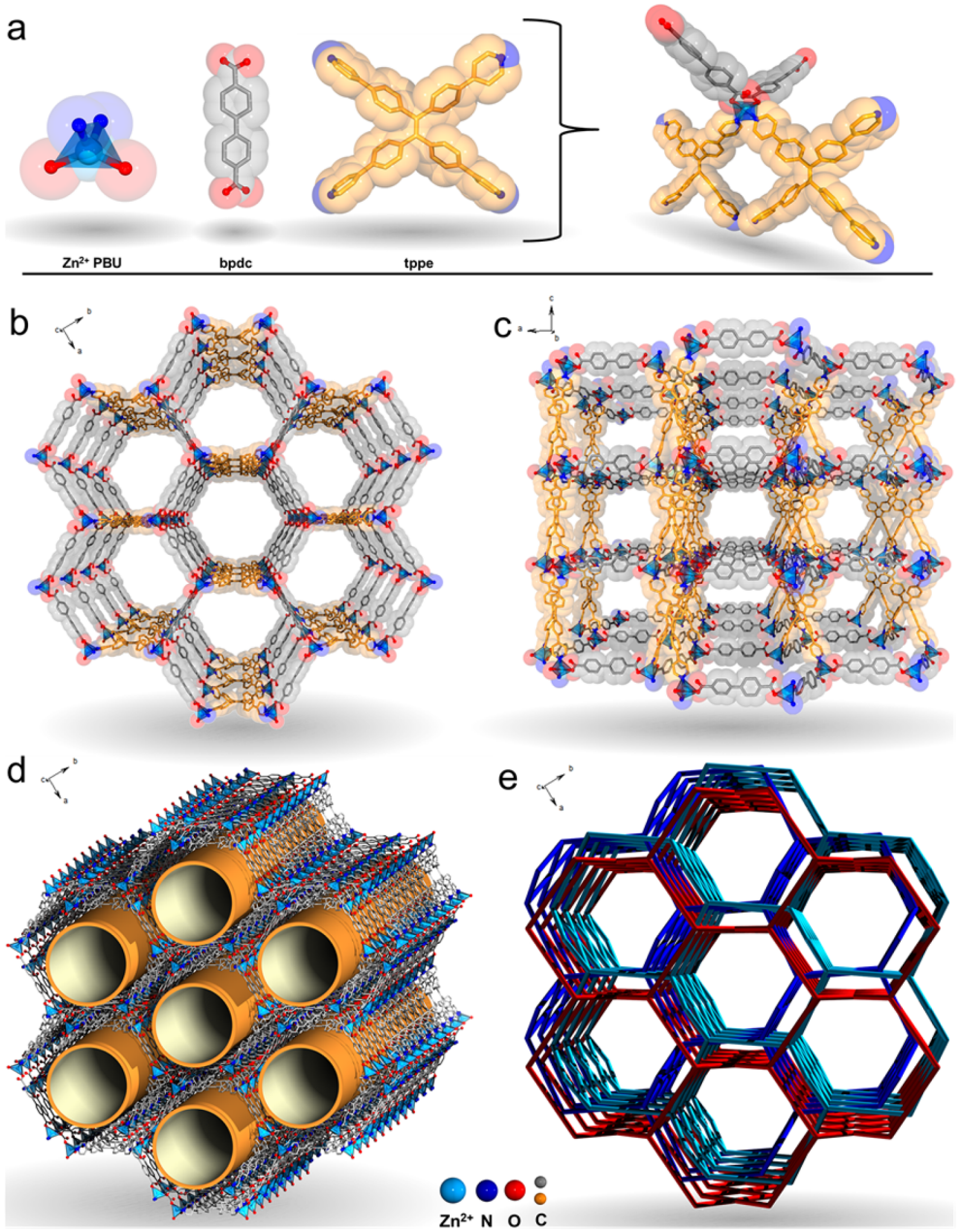

Figure 2. (a) PBU of LMOF-241, showcasing a tetrahedrally coordinated Zn center bound to two tppe molecules and two bpdc molecules. (b) Single net of LMOF-241 framework viewed along the *c* -axis, composed of edge-sharing hexagonal channels. (c) Single net of LMOF-241 framework viewed along the *b*-axis, showing pores that are closed upon the interpenetration. (d) Overall crystal structure demonstrating the three-fold interpenetration and 1D pore running along the *c*-axis. (e) LMOF-241 drawn as 2-nodal (4,4)-c net (mog-type), with tppe and bpdc simplified as a 4-c node and 2-c node, respectively. The different colors (red, blue, and aqua) indicate the three distinct interpenetrated networks that form the complete structure of LMOF-241. In all structures, H atoms are omitted for clarity.

(Figure 2b). The overall structure of LMOF-241 is a three-fold interpenetrated framework formed by three of these identical nets, with distorted hexagonal 1D channels of diameter ~16.6 Å along the *c*-axis (Figure 2d). If bpdc is simplified as a 2-c node and tppe as a 4-c node, the framework would be a 2-nodal (4,4)-c net (mog-type) with point symbol $\{4\cdot6^4\cdot8\}_2\{4^2\cdot6^2\cdot8^2\}$ (Figure 2e). There are currently 12 reported MOF structures with three-fold interpenetrated mog-type topology according to the ToposPro database.[15] If tppe is simplified as two 3-c nodes, the framework would be a 2-nodal (3,4)-c net (jeb-type, or bbe-3,4-*Cmmm*, derived from mog) with point symbol $\{6^3\}\{6^5\cdot8\}$.[16] To the best of our knowledge, only 1 out of all 8 reported jeb-type MOF structures has a three-fold interpenetration.[17] However, the topology of LMOF-241 is unusual because of its noncentrosymmetry: two structural groups not related by any symmetry operations form 3 (2 + 1) interpenetrated nets.

Optical Properties of LMOF-241. The UV−vis reflectance spectra of the ligand tppe and LMOF-241 were collected using a Shimadzu UV-3600 spectrophotometer, after which conversion to the Kubelka−Munk function allowed their optical band gaps to be estimated. The estimated optical HOMO−LUMO gaps are 2.3 and 2.6 eV for tppe and LMOF-241, respectively (Figure S4). Photoluminescence excitation and emission spectra were collected for samples of tppe and

DOI: 10.1021/jacs.5b10308
J. Am. Chem. Soc. 2015, 137, 16209−16215

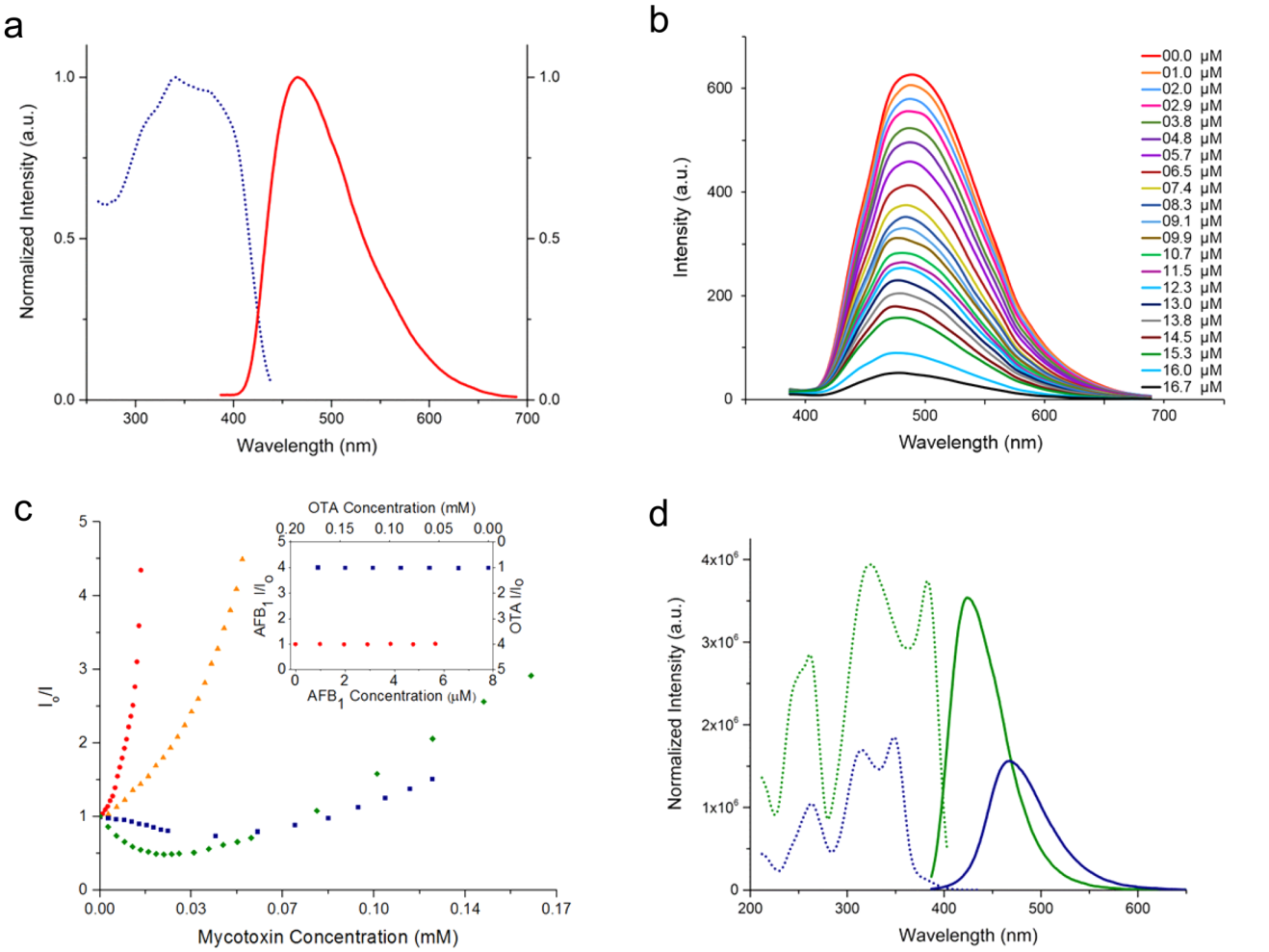

Figure 3. (a) Excitation (dotted blue) and emission (solid red, λ_{ex} = 340 nm) spectra of LMOF-241 suspended in DCM. (b) Emission spectra of LMOF-241 with the incremental addition of AFB_1 in DCM, with toxin concentrations given in the key to the right of the figure. (c) Stern−Volmer curves acquired at λ_{ex} = 340 nm and λ_{ex} = 410 nm (inset) for AFB_1 (red dot), AFB_2 (orange triangle), AFG_1 (green diamond), and OTA (blue square). (d) Excitation (dotted lines) and emission (solid lines, λ_{ex} = 340 nm) spectra of AFG_1 (green) and OTA (blue) in DCM with intensity normalized to concentration.

LMOF-241 at room temperature. Both samples showed strong blue-green emission when excited by UV light (λ_{ex} = 340 nm), with tppe having an emission maximum at 490 nm, while that of LMOF-241 was slightly red-shifted to 500 nm (Figure S5). In designing LMOF-241, we desired to preserve the strong emission from the tppe ligand in the final structure. Specifically, the immobilization of the chromophore ligand in the MOF framework would not alter the nature of ligand-based emission. The Zn^{2+} ion was chosen for this purpose because, as a d^{10} metal with low-lying d-orbital energies, it is known to contribute negligibly in the luminescence of the resulting LMOFs.[13,19,20]

A Hamamatsu C9220-03 spectrophotometer with integrating sphere was used to determine the IQY of both samples at 360 nm excitation. The values are 76.7 and 92.7% for tppe and LMOF-241, respectively. To the best of our knowledge, the latter represents the highest value reported so far for green-emitting MOFs. The significant increase (16%) in quantum yield is consistent with previous findings, indicating that immobilizing molecular chromophores (such as tppe) into rigid frameworks can improve the material's fluorescence efficiency by eliminating nonradiative relaxation pathways such as some vibrational and rotational motions.[13,18,19] The high efficiency makes LMOF-241 an excellent candidate as fluorescence-based sensory material.

Mycotoxin Detection. Mycotoxin detection was achieved by monitoring the PL signal change of the LMOF-241 suspension before and after the addition of the analyte. Upon addition of the mycotoxins, the emission in intensity of LMOF-241 was quenched. A representative set of PL titration curves for AFB_1 are shown in Figure 3b, demonstrating that the degree of quenching increases as a function of AFB_1 concentration. The quenching efficiency was quantified using the Stern−Volmer (SV) equation:

$$I_0/I = K_{SV}[Q] + 1$$

I_0 is the initial emission peak intensity, I is the emission peak intensity after the addition of analyte, $[Q]$ is molar concentration of the analyte (quencher), and K_{SV} is the quenching efficiency, which was used to quantitatively evaluate the performance of LMOF-241 as mycotoxin sensor. As shown in Figure 3c, at low concentrations, the I_0/I is linearly proportional to concentration for both AFB_1 and AFB_2; the slope is the K_{SV}. The K_{SV} plots for AFG_1 and OTA are also shown in Figure 3c.

DOI: 10.1021/jacs.5b10308
J. Am. Chem. Soc. 2015, 137, 16209−16215

For AFB_1, K_{SV} is 54 227 M^{-1}, which is among the highest values reported for the known sensory materials. This value is also nearly twice that of AFB_2 (32 436 M^{-1}), indicating a high selectivity of LMOF-241 toward AFB_1. The detection limit for AFB_1 is estimated to be 46 ppb, significantly better than 300 ppb, the tolerant level set by the FDA for corn and peanut feeds for beef cattle.[20] The SV curves for AFG_1 and OTA bend downward first at low concentration region, and this trend is reversed after certain concentration thresholds. This is because both AFG_1 and OTA are fluorescent under 340 nm excitation, while both AFB_1 and AFB_2 are nonfluorescent under the same conditions. As a result, at low concentration, these two toxins add to the overall emission intensity, causing a decrease in their SV curves. However, once a certain concentration threshold is reached, interactions between the toxins and LMOF-241 lead to a net quenching. Compared to OTA, AFG_1 emits more efficiently and also acts as a stronger quencher, as evident from the shape of both slopes. The threshold concentration from PL enhancement to quenching of AFG_1 is also lower than that of OTA. In addition to intensity change, AFG_1 causes a blue shift of the emission peak while OTA gives a red shift. Such turn-on and turn-off responses are unique fingerprints of these two mycotoxins.

Mycotoxin Detection Mechanism. The quenching of LMOF-241's emission by AFB_1 and AFB_2 is likely due to an electron transfer mechanism that we previously discussed for LMOF-based sensors.[19] Based on the results obtained from our molecular orbital calculations (see S10, Table S1), the bottom of the LUMO (or CB) energy states of LMOF-241 lies above the LUMO energies of AFB_1 and AFB_2, allowing an efficient electron transfer from the MOF to both toxin molecules (Figure 4). In addition, the LUMO of AFB_1 is lower in energy

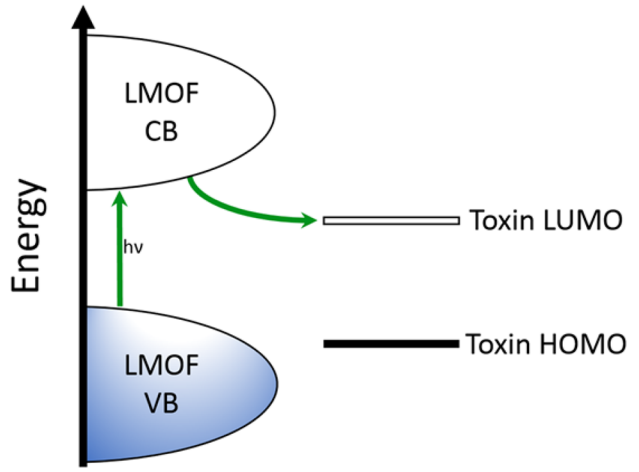

Figure 4. Schematic demonstrating electron transfer from LMOF-241 to mycotoxin LUMO, resulting in quenched emission.

compared to that of AFB_2, which accounts for its stronger tendency of such electron transfer and higher degree of quenching effect.

The extent of analyte−sensor interactions also plays an important role in the electron transfer process. With LMOF-241's channel diameter being approximately 16.6 Å, we expect that the Aflatoxin molecules (measuring approximately 13.3 Å at their widest) would be able to enter the pores. To confirm this and quantitatively assess the analyte−sensor interactions, we first carried out a structure optimization process on AFB_1 and AFB_2-loaded LMOF-241, using the Materials Studio Sorption Package, which utilized the GCMC method and Burchard universal force field. Analyte sites located within the LMOF pore with the shortest distances to the MOF were identified for each of AFB_1 and AFB_2 by the GCMC simulation method (see S9, Figure S9 and Figure S10). We then performed overlap population calculations using the EH method to quantitatively measure such interactions. The absolute fragment molecular orbital overlap population (SAFMOOP) and absolute reduced overlap population (AROP) between the analytes and the MOF were obtained (see S10 and Table S2). The average of the summed absolute orbital overlap between AFB_1 and LMOF-241 is 0.57, whereas that between AFB_2 and LMOF-241 is 0.17, indicating that AFB_1 interacts significantly stronger with the MOF framework than AFB_2. The reduced overlap population follows the same order, with the AFB_1 value 1.4 times that for AFB_2. The stronger orbital overlap of AFB_1 with LMOF-241 is due to the higher π-conjugation of AFB_1, creating more π-type overlap with the conjugate π-orbitals of LMOF-241. As a result, it facilitates a more efficient electron transfer and a higher extent of fluorescence quenching.

Energy transfer often contributes significantly in fluorescence quenching and should also be considered. As can be seen in Figure 5a, the spectral overlap between the mycotoxin absorption and LMOF-241 emission is very limited, which hinders the energy transfer from LMOF-241 to AFB_1 and AFB_2,[20] indicating that it does not likely play a role in the mycotoxin detection. However, when comparing the excitation spectrum of LMOF-241 with the emission spectra of AFG_1 and OTA (note: AFB_1 and AFB_2 are nonemissive), it is apparent that there is significant overlap, especially in the case of AFG_1 (Figure 5c). The energy transfer between the excited toxins (AFG_1 and OTA) and LMOF-241 is likely to contribute appreciably to the apparent increase in the fluorescence intensity of LMOF-241 at low concentrations of AFG_1 and OTA (Figure 3c). AFG_1 causes a higher degree of increase in LMOF-241 fluorescence intensity, as its emission overlaps more strongly with LMOF-241's excitation spectrum than that of OTA.

Also noted in Figure 5a is that all four mycotoxins absorb the excitation energy used in the sensing experiment (λ_{ex} = 340 nm). This suggests that competition between the MOF and the toxins for excitation energy may also contribute to the quenching of LMOF-241's emission. However, it is unlikely that competition for excitation energy plays a significant role in the observed emission quenching, as the toxins are present in extremely low amounts relative to LMOF-241 throughout the sensing titration. Additionally, if competition for excitation energy was occurring to a significant degree, nonspecific quenching of any fluorophores under 340 nm excitation in the presence of the mycotoxins would be observed. Figure 5b demonstrates that luminescence from the tppe linker, itself a strong fluorophore, is not affected by titration with AFB_1. The strong and continuing decrease in LMOF-241 emission intensity is primarily due to the electron transfer process described above.

Figure 5b also reveals that incorporating the fluorophore into a metal−organic framework is vital for the selective emission quenching to occur. While the tppe molecule is a strong fluorophore, it does not strongly interact with the toxin molecules. By anchoring the fluorophore into a crystalline, porous framework using the metal oxide PBU, we create a well-

DOI: 10.1021/jacs.5b10308
J. Am. Chem. Soc. 2015, 137, 16209−16215

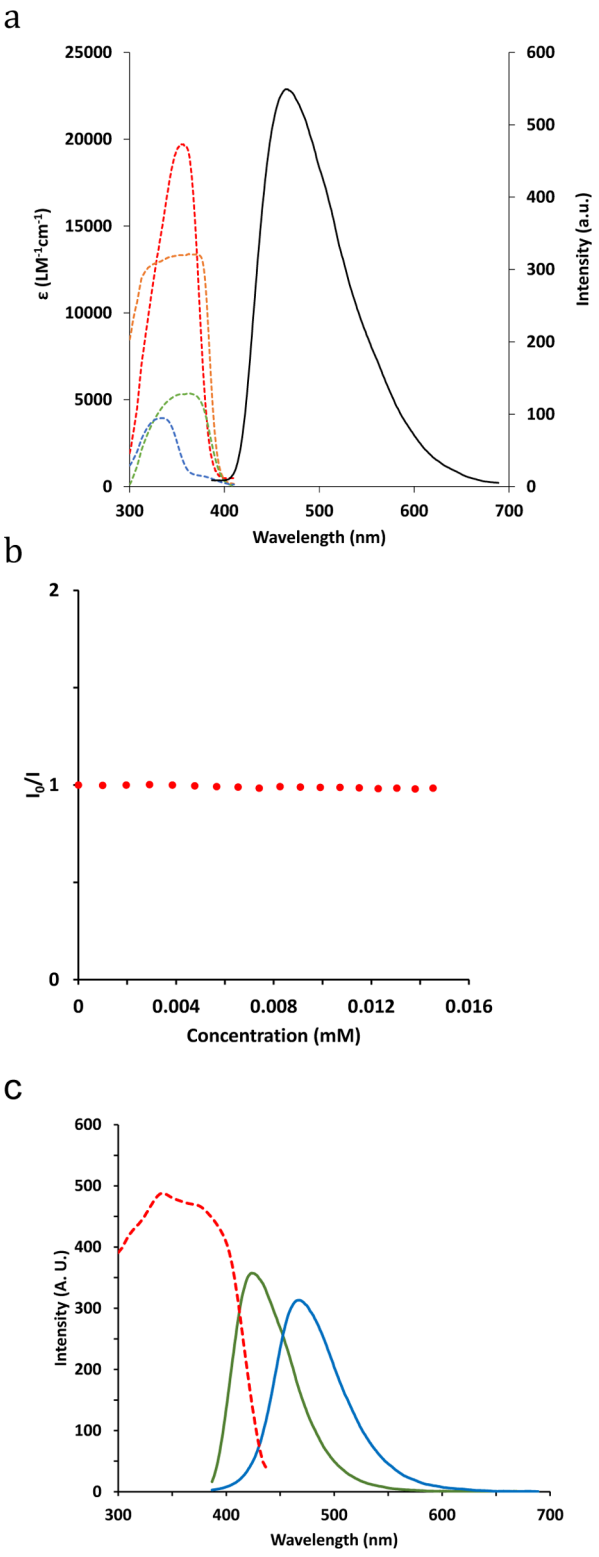

Figure 5. (a) Molar absorptivity of AFB_1 (dotted red), AFB_2 (dotted orange), AFG_1 (dotted green), and OTA (dotted blue), and the emission spectrum of LMOF-241 in DCM (solid black, λ_{ex} = 340 nm). (b) K_{SV} plot for the titration of a 4 mg/mL solution of tppe with AFB_1. (c) Excitation spectrum of LMOF-241 in DCM (dotted red) overlaid on the emission spectra (solid lines, λ_{ex} = 340 nm) of AFG_1 (green) and OTA (blue) in DCM.

characterized material that has both an intense emission signal and a strong interaction with the target mycotoxins.

CONCLUSIONS

We have designed and synthesized a new luminescent MOF and investigated its luminescent properties as well as related applications in chemical sensing. LMOF-241 is a blue-green emitting LMOF with an exceptionally high internal quantum yield (92.7%). We have demonstrated for the first time the use of this compound for the effective and selective optical detection of mycotoxins via a luminescence quenching mechanism. LMOF-241 is capable of quickly and efficiently detecting and differentiating several major Aflatoxins and Ochratoxin A and is most sensitive toward Aflatoxin B_1. With a detection limit of 46 ppb, LMOF-241 makes one of the best performing luminescence-based chemical sensors to date. We have also studied the electronic properties of LMOF-241 and the selected mycotoxins by theoretical methods. A possible detection mechanism via electron, rather than energy, transfer processes is elucidated. These results suggest that LMOFs have immense potential as simple, low-cost, easily portable, and readily available luminescence-based sensors for the detection of biochemical hazards such as toxins and other toxic molecular species, which can be particularly useful for developing countries. This study opens a new direction for practical applications making use of multifunctional MOFs.

ASSOCIATED CONTENT

Supporting Information

The Supporting Information is available free of charge on the ACS Publications website at DOI: 10.1021/jacs.5b10308.

PXRD, TGA, computation details (PDF)
X-ray data (CIF)

AUTHOR INFORMATION

Corresponding Author

*jingli@rutgers.edu

Author Contributions

‖Z.H. and W.P.L. contributed equally.

Notes

The authors declare no competing financial interest.

ACKNOWLEDGMENTS

The Rutgers team is grateful for the financial support from the Materials Sciences and Engineering Division, Office of Basic Energy Sciences, of the U.S. Department of Energy through Grant No. DE-FG02-08ER-46491. The Advanced Light Source is supported by the Director, Office of Science, Office of Basic Energy Sciences, of the U.S. Department of Energy under Contract No. DE-AC02-05CH11231. Z.H. would like to thank Prof. Davide M. Proserpio for his insightful analysis of the structure topology. W.P.L. would like to thank Ben Deibert for his invaluable assistance with the structure images, as well as general feedback and discussion.

REFERENCES

(1) Al-Taher, F.; Banaszewski, K.; Jackson, L.; Zweigenbaum, J.; Ryu, D.; Cappozzo, J. *J. Agric. Food Chem.* **2013**, *61*, 2378.
(2) Schmale, D. G., III; Munkvold, G. P. *The Plant Health Instructor*, 2009. http://www.apsnet.org/edcenter/intropp/topics/Mycotoxins/Pages/default.aspx (accessed Mar 16, 2015).
(3) USFDA *Compliance Program Guidance Manual*, 2007.
(4) Bhat, R.; Rai, R. V.; Karim, A. A. *Compr. Rev. Food Sci. Food Saf.* **2010**, *9*, 57.
(5) Shephard, G. S. *Chem. Soc. Rev.* **2008**, *37*, 2468.

DOI: 10.1021/jacs.5b10308
J. Am. Chem. Soc. 2015, 137, 16209−16215

(6) Song, S.; Liu, N.; Zhao, Z.; Njumbe Ediage, E.; Wu, S.; Sun, C.; De Saeger, S.; Wu, A. *Anal. Chem.* **2014**, *86*, 4995.
(7) Yue, S.; Jie, X.; Wei, L.; Bin, C.; Dou Dou, W.; Yi, Y.; QingXia, L.; JianLin, L.; TieSong, Z. *Anal. Chem.* **2014**, *86*, 11797.
(8) USFDA *CPG Sec. 683.100 Action Levels for Aflatoxins in Animal Feeds*, 2014.
(9) You, L.; Zha, D.; Anslyn, E. V. *Chem. Rev.* **2015**, *115*, 7840.
(10) Basabe-Desmonts, L.; Reinhoudt, D. N.; Crego-Calama, M. *Chem. Soc. Rev.* **2007**, *36*, 993.
(11) (a) Nugent, P.; Belmabkhout, Y.; Burd, S. D.; Cairns, A. J.; Luebke, R.; Forrest, K.; Pham, T.; Ma, S.; Space, B.; Wojtas, L.; Eddaoudi, M.; Zaworotko, M. J. *Nature* **2013**, *495*, 80. (b) Choi, K. M.; Na, K.; Somorjai, G. A.; Yaghi, O. M. *J. Am. Chem. Soc.* **2015**, *137*, 7810. (c) Fracaroli, A. M.; Furukawa, H.; Suzuki, M.; Dodd, M.; Okajima, S.; Gandara, F.; Reimer, J. A.; Yaghi, O. M. *J. Am. Chem. Soc.* **2014**, *136*, 8863. (d) Sasan, K.; Lin, Q.; Mao, C.; Feng, P. *Chem. Commun.* **2014**, *50*, 10390. (e) Zhao, X.; Wong, M.; Mao, C.; Trieu, T. X.; Zhang, J.; Feng, P.; Bu, X. *J. Am. Chem. Soc.* **2014**, *136*, 3252. (f) Ma, S.; Sun, D.; Ambrogio, M.; Fillinger, J. A.; Parkin, S.; Zhou, H.-C. *J. Am. Chem. Soc.* **2007**, *129*, 1858.
(12) (a) Zhang, S. H.; Shi, W.; Cheng, P.; Zaworotko, M. J. *J. Am. Chem. Soc.* **2015**, *137*, 12203. (b) Hu, Z.; Deibert, B. J.; Li, J. *Chem. Soc. Rev.* **2014**, *43*, 5815. (c) Banerjee, D.; Hu, Z.; Li, J. *Dalton Transactions* **2014**, *43*, 10668.
(13) Gong, Q.; Hu, Z.; Deibert, B. J.; Emge, T. J.; Teat, S. J.; Banerjee, D.; Mussman, B.; Rudd, N. D.; Li, J. *J. Am. Chem. Soc.* **2014**, *136*, 16724.
(14) (a) Hoffman, R. *J. Chem. Phys.* **1963**, *39*. (b) Whangbo, M. H.; Hoffmann, R.; Woodward, R. B. *Proc. R. Soc. London* **1979**, *A366*.
(15) Blatov, V. A.; Shevchenko, A. P.; Proserpio, D. M. *Cryst. Growth Des.* **2014**, *14*, 3576.
(16) (a) Blatov, V. A.; Proserpio, D. M. *Acta Crystallogr., Sect. A: Found. Crystallogr.* **2009**, *65*, 202. (b) Li, M.; Li, D.; O'Keeffe, M.; Yaghi, O. M. *Chem. Rev.* **2014**, *114*, 1343.
(17) Farnum, G. A.; LaDuca, R. L. *Cryst. Growth Des.* **2010**, *10*, 1897.
(18) Wei, Z.; Gu, Z.-Y.; Arvapally, R.; Chen, Y.-P.; McDougald, R.; Yakovenko, A.; Feng, D.; Omary, M.; Zhou, H.-C. *J. Am. Chem. Soc.* **2014**, *136*, 8269.
(19) (a) Pramanik, S.; Zheng, C.; Zhang, X.; Emge, T. J.; Li, J. *J. Am. Chem. Soc.* **2011**, *133*, 4153. (b) Hu, Z.; Pramanik, S.; Tan, K.; Zheng, C.; Liu, W.; Zhang, X.; Chabal, Y. J.; Li, J. *Cryst. Growth Des.* **2013**, *13*, 4204. (c) Pramanik, S.; Hu, Z.; Zhang, X.; Zheng, C.; Kelly, S.; Li, J. *Chem. - Eur. J.* **2013**, *19*, 15964. (d) Banerjee, D.; Hu, Z.; Pramanik, S.; Zhang, X.; Wang, H.; Li, J. *CrystEngComm* **2013**, *15*, 9745.
(20) Hu, Z.; Tan, K.; Lustig, W. P.; Wang, H.; Zhao, Y.; Zheng, C.; Banerjee, D.; Emge, T. J.; Chabal, Y. J.; Li, J. *Chemical Science* **2014**, *5*, 4873.

DOI: 10.1021/jacs.5b10308
J. Am. Chem. Soc. 2015, 137, 16209−16215